Hindawi
Shock and Vibration
Volume 2021, Article ID 4431516, 18 pages
https://doi.org/10.1155/2021/4431516

Research Article

Vortex-Induced Vibration Suppression of Bridges by Inerter-Based Dynamic Vibration Absorbers

Junjie Chen,[1] Michael Z. Q. Chen ,[1] and Yinlong Hu [2]

[1]*School of Automation, Nanjing University of Science and Technology, Nanjing 210094, China*
[2]*College of Energy and Electrical Engineering, Hohai University, Nanjing 211100, China*

Correspondence should be addressed to Michael Z. Q. Chen; mzqchen@outlook.com

Received 26 April 2021; Revised 10 June 2021; Accepted 17 June 2021; Published 6 July 2021

Academic Editor: Yan Han

The vortex-induced vibration may cause fatigue of a bridge structure, affecting the safety of vehicles and the comfort of pedestrians. Inerter is a two-terminal device, which has been applied in many areas. This paper studies the problem of suppressing the vortex-induced vibration of a bridge by using an inerter-based dynamic vibration absorber (IDVA). The performances in terms of the suspension travel and the vertical displacement of the bridge with different IDVAs in suppressing vortex-induced vibration are compared, and the effect of the installation position of IDVA on the performance of suppressing vortex-induced vibration is shown. The performance indexes for the vertical displacement of six IDVA arrangements are obtained by using an iterative method, where the performance indexes for the vertical displacement are minimized by using the optimization toolbox in a commercial software. The result shows that the optimal installation positions and the number of suitable installation positions are affected by the resonant mode. Among the six arrangements, one arrangement is identified to have the best performance of suppressing vortex-induced vibration. All the six arrangements have reduced the suspension travel performance.

1. Introduction

With the development of the construction technology, the lengths of bridges have become longer, making the bridges more sensitive to wind-induced vibrations. The vortex-induced vibration is a type of wind-induced vibration, which often occurs at a low wind velocity. When wind blows through slender structures like a bridge, the double-row line vortex with the opposite direction of rotation and regular arrangement is periodically dropped on the upper and lower sides. This phenomenon is referred to as the Karman Vortex Street [1]. Vibration will occur as the Karman Vortex Street alternately falls off, and resonance occurs when the shedding frequency is close to the natural frequency of a bridge. Sustained vibration can cause fatigue of the bridge structure, affecting the safety of vehicles and the comfort of pedestrians. Therefore, the research on vortex-induced vibration has become a very active topic for scholars [2–7].

The main measures to suppress vortex-induced vibration are divided into aerodynamic measures and mechanical measures. Aerodynamic measures mainly improve the aerodynamic shape of the structure to avoid vortex-induced vibration. Zhou et al. [8] studied the effects of bridge attachments such as sidewalks, railings, and crash barriers on the suppression of vortex-induced vibrations by the means of numerical simulation and wind tunnel tests. A passive vortex generator was used to avoid the stability of vortex shedding for the purpose of suppressing vortex-induced vibration [9]. The mechanical measure is to suppress the vortex-induced vibration of a bridge by using a mechanical energy absorption system in the bridge. A commonly used mechanical equipment is the tuned mass damper, referred to as TMD (or dynamic vibration absorber, DVA). In 2002, TMD was used to suppress the vortex-induced vibration of Rio-Niteroi bridge [10] and Trans-Tokyo Bay Crossing bridge [11]. Multiple tuned mass dampers (MTMD) were used to suppress the high-order vortex-induced vibration of the suspension bridge [12].

Inerter, a new type of mechanical device, was proposed by Smith [13], as shown in Figure 1. The inerter is defined as

a two-terminal mechanical element whose force acting on two terminals is proportional to the relative acceleration of two terminals, where the proportionality coefficient is referred to as the inertance. According to the definition, the dynamic equation of inerter is

$$F = b(\dot{v}_1 - \dot{v}_2), \tag{1}$$

where F is the force acting on two terminals, v_1 and v_2 are the velocities of two terminals, and b is the inertance.

With the force-current analogy, the damper, spring and inerter in a passive mechanical network are analogous to the resistor, inductor, and capacitor in a passive electrical network. The inerter was first applied in the field of network synthesis [14]. Any controllers with positive real admittance functions can be realized by interconnections of inerters, dampers, and springs [15]. At present, inerter has become an active topic for many scholars. Meanwhile, the concept of semi-active inerter was also proposed and its physical realizations were established [16].

The inerter has been used to suppress wind-induced vibration of cables in cable-stayed bridges. A variety of given network arrangements [17–19] and the network comprehensive solution [20] have been used to design IDVAs, where the minimum modal damping of the stay cable was effectively improved. Xu et al. [21] used inerter to suppress the vortex-induced vibration of a bridge, where the minimum RMS value of the bridge displacement was obtained. Dai et al. [22] studied the effect of installation position of the inerter on the damping performance of the inerter-based tuned mass damper (TMDI) to suppress the wind-induced vibration of the flexible structure.

In 2015, Hu and Chen [23] proposed the inerter-based dynamic vibration absorbers, as shown in Figure 2(a), which are different from the traditional dynamic vibration absorber. The traditional dynamic vibration absorber, usually referred to as TDVA or TMD, can be composed of dampers and springs, as shown in Figure 2(b). However, the inerter-based dynamic vibration absorbers can be composed of dampers, springs, and inerters. IDVAs have been used to control the seismic response of a steel building structure [24]. Mechanical schematic diagram of IDVA used in [24] is shown in Figure 3, which can be applied to other buildings.

Six arrangements were used to design IDVAs in [23]; see C1-C6 arrangements shown in Figure 4. The performances of IDVAs were measured from the perspective of the H_∞ norm and H_2 norm of the system. The H_2 norm optimization problem in [23] was equivalent to a white noise excitation problem. It was found that in the H_2 norm optimization the performance of C3 arrangement was the best, followed by C6 and C4, and the worst one was C5.

In 2019, Xu et al. [21] applied the inerter to suppress the vortex-induced vibration of bridges and named the device as the inerter-based tuned mass damper (TMDI). The TMDI was installed inside a bridge, and the parameters were tuned to minimize the RMS value of the displacement of a bridge. It was shown that better vortex-induced vibration suppression performance would be achieved with a larger mass ratio and a smaller inertance-to-mass ratio. However, it was found that the performance deteriorates after adding the inerter compared with the traditional arrangement.

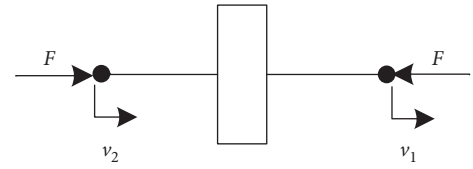

Figure 1: Symbolic representation of inerter.

The similarities and differences between [23] and [21] are as follows. Firstly, the arrangement in [21] is the C1 arrangement mentioned in [23]. In addition, the excitations are different. The H_2 norm performance in [23] is equivalent to a white noise excitation problem; while colored noises are employed in [21]. It was found that the performance of the C1 arrangement in suppressing vortex-induced vibration was inferior to the traditional arrangement in [21], consistent with the conclusion in [23]. In 2020, Xu et al. [25] compared the performance of C2-C4 arrangements in suppressing vortex-induced vibration. The parameters of each arrangement were selected based on the H_2 performance indices in [23].

Note that the application of inerter in a beam was studied in [26]. The difference is that the excitation studied in [26] is the frequency-bounded white noise, which only acts at a point on the beam and belongs to point excitation. In this paper, the excitation acts on any point of the beam and belongs to distributed excitation.

This paper studies the vortex-induced vibration suppression problem of bridges by using the inerter-based dynamic vibration absorber (IDVA). The performances of different IDVAs in suppressing vortex-induced vibration are compared, and the effect of the installation position on the performance of suppressing vortex-induced vibration is analyzed. This paper uses C3-C6 arrangements in [23] and C7-C8 arrangements in [27] to form IDVAs. Different from the study in [21], the installation location of the IDVA is emphasized in this paper, where a Euler–Bernoulli beam is adopted to model the bridge. The bridge-IDVA equivalent model studied in the paper is shown in Figure 5.

2. Bridge-IDVA Mathematical Model

Since other IDVA arrangements can be similarly obtained, the C4 arrangement is selected to illustrate the procedure of establishing the bridge-IDVA model. Actually, all the mathematical models of other IDVA arrangements can be similarly established, where the details are not shown in this paper for brevity. The C4 arrangement of IDVA is installed inside a bridge, as shown in Figure 6. A Euler–Bernoulli model of the bridge with the IDVA installed at the point $x = a$ is shown in Figure 7.

The dynamic equations of motion of the bridge-IDVA system are as follows:

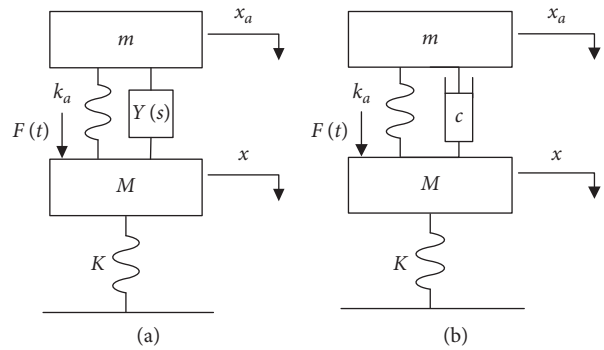

Figure 2: Dynamic vibration absorber. (a) Inerter-based dynamic vibration absorber; (b) traditional dynamic vibration absorber.

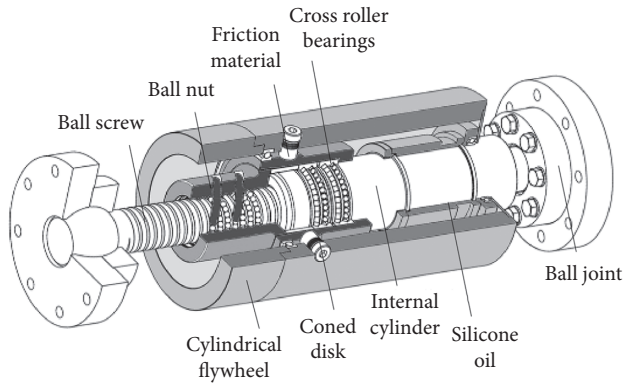

Figure 3: Mechanical schematic diagram of IDVA.

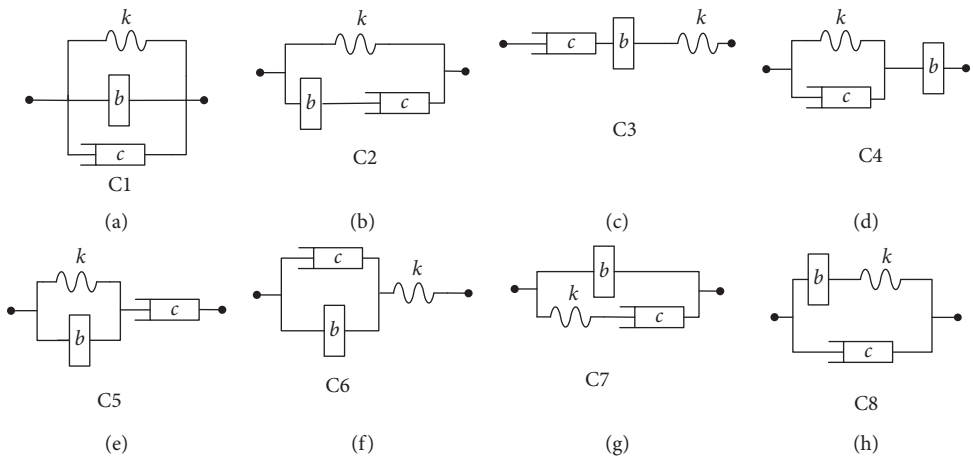

Figure 4: Eight passive mechanical networks with a spring, a damper, and an inerter.

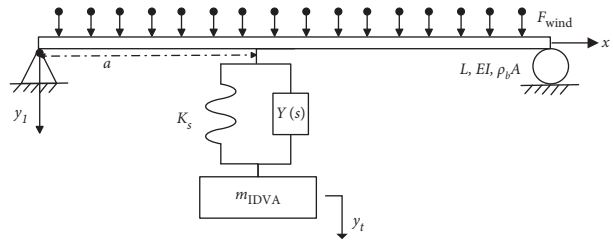

Figure 5: The simplified bridge-IDVA model.

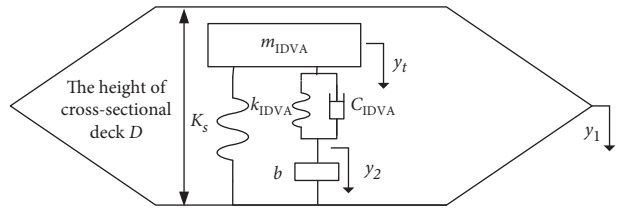

Figure 6: The installation of IDVA.

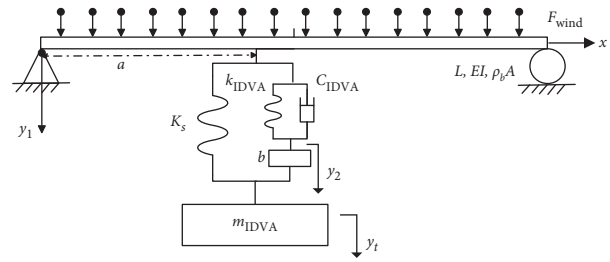

Figure 7: The simplified bridge-IDVA system with C4 arrangement.

$$\rho_b A \frac{\partial^2 y_1(x,t)}{\partial t^2} + m_{\text{IDVA}} \frac{\partial^2 y_t(t)}{\partial t^2} \delta(x-a) + c \frac{\partial y_1(x,t)}{\partial t} + EI \frac{\partial^4 y_1(x,t)}{\partial x^4} = F_{\text{wind}},$$
$$F_{\text{wind}} = \frac{1}{2}\rho U^2 D \left[Y_1 \left(1 - \varepsilon \frac{y_1(x,t)^2}{D^2} \right) \frac{(\partial y_1(x,t)/\partial t)}{U} + Y_2 \frac{y_1(x,t)}{D} \right] + \frac{1}{2}\rho U^2 D \widetilde{C}_L(x,t), \tag{2}$$

$$m_{\text{IDVA}} \frac{\partial^2 y_t(t)}{\partial t^2} = b\left(\frac{\partial^2 y_2(t)}{\partial t^2} - \frac{\partial^2 y_t(t)}{\partial t^2} \right) + K_s \left(y_1(a,t) - y_t(t) \right), \tag{3}$$

$$b\left(\frac{\partial^2 y_2(t)}{\partial t^2} - \frac{\partial^2 y_t(t)}{\partial t^2} \right) = c_{\text{IDVA}} \left(\frac{\partial y_1(a,t)}{\partial t} - \frac{\partial y_2(t)}{\partial t} \right) + k_{\text{IDVA}} \left(y_1(a,t) - y_2(t) \right), \tag{4}$$

where $y_1(x,t)$ is the vertical displacement of the bridge, $y_t(t)$ is the displacement of the mass m_{IDVA}, $y_2(t)$ is the displacement of the connection between the inerter and the spring (or the damper), U is the mean wind velocity, D is the height of cross sectional deck, c is the structural damping, EI is the flexural rigidity of the bridge, $\rho_b A$ is the mass per unit length of the bridge, ρ is the air density, Y_1, Y_2, and ε are aeroelastic parameters that can be obtained from a wind tunnel test, $\widetilde{C}_L(x,t)$ is the lift coefficient. $\delta(x-a) = \begin{cases} 1 & x = a \\ 0 & x \neq a \end{cases}$ is the Dirac delta function, and F_{wind} is the vortex-induced force.

By using the Galerkin method [28], the vertical displacement of the bridge can be obtained as

$$y_1(x,t) = \sum_{1}^{n} \phi_j(x) q_j(t), \tag{5}$$

in which $q_j(t)$ is a function of model coordinate and $\phi_j(x)$ is the jth modal function of a simply supported beam and can be determined by solving the eigenvalue problem with a certain boundary condition. $\int_0^L \phi_j(x)\phi_k(x)\mathrm{d}x = L\delta_{jk}$ and $(\mathrm{d}^4\phi_j(x))/\mathrm{d}x^4 = \tau_j^4\phi_j(x)$ are satisfied, where τ_j is the eigenvalue of the beam characteristic equation, L is the length of the bridge, and δ_{jk} is the Kronecker delta function.

When the frequency of vortex shedding is similar to the natural frequency of one bridge mode, the frequency of vortex shedding is captured by the natural frequency. This phenomenon is referred to as "lock in" [1]. In the "lock in" region, the vortex resonates with only one mode of the bridge. Thus, the vertical displacement of the bridge can be simplified as follows:

$$y_1 = \phi_i(x) q_i(t), \tag{6}$$

where $\phi_i(x)$ is the modal function of resonance mode.

Substituting (6) into equations (2)–(4), and moving the part of the vortex-induced force related to the vertical displacement and velocity of the bridge to the left side of the equation, after introducing the dimensionless parameters, the equations of motion of the system can be rewritten as

$$\begin{aligned} M_i\ddot{q}_i(t) + \mu M_i\phi_i(a)\ddot{y}_t + 2M_i\omega_i(\xi_i - \xi_{\mathrm{ae}})\dot{q}_i(t) + \left(M_i\omega^2{}_i - K_{\mathrm{ae}}\right)q_i(t) = F_i, \\ F_i = \frac{1}{2}\rho U^2 D\int_0^L \widetilde{C}_L(x,t)\phi_i(x)\mathrm{d}x, \end{aligned} \tag{7}$$

$$\mu\ddot{y}_t - \beta(\ddot{y}_2 - \ddot{y}_t) - \mu\omega_s{}^2(\phi_i(a)q_i(t) - y_t) = 0, \tag{8}$$

$$\beta(\ddot{y}_2 - \ddot{y}_t) - 2\mu\xi_T\omega_S(\phi_i(a)\dot{q}_i(t) - \dot{y}_2) - \mu\omega_T{}^2(\phi_i(a)q_i(t) - y_2(t)) = 0, \tag{9}$$

where F_i is the excitation related to the lift coefficient, $M_i = \rho_b A\int_0^L \phi_i(x)^2\mathrm{d}x$ is the modal mass, $\omega_i = \sqrt{(EI\tau_i^4/\rho_b A)}$ is the modal frequency, $\xi_i = (c/(2\sqrt{EI\tau_i^4\rho_b A}))$ is the modal damping ratio, $\omega_s = \sqrt{K_s/m_{I\ DV\ A}}$ is the natural frequency of the IDVA, $\omega_T = \sqrt{k_{\mathrm{IDVA}}/m_{\mathrm{IDVA}}}$ is the corner frequency of the IDVA, $\xi_T = (c_{\mathrm{IDVA}})/(2\sqrt{m_{\mathrm{IDVA}}K_s}))$ is the damping ratio of the IDVA, $\mu = (m_{\mathrm{IDVA}}/M_i)$ is the mass ratio, $\beta = b/M_i$ is the inertance-to-mass ratio, ξ_{ae} is the aeroelastic damping, and K_{ae} is the aeroelastic stiffness, ξ_{ae} and K_{ae} can be calculated as

$$\begin{aligned} \xi_{\mathrm{ae}} &= \frac{\rho U\ DY_1}{4M_i\omega_i}\left(\int_0^L \phi_i(x)^2\mathrm{d}x - \frac{\varepsilon\int_0^L \phi_i(x)^4\mathrm{d}x}{D^2}q_i^2(t)\right), \\ K_{\mathrm{ae}} &= \frac{\rho U^2 DY_2}{2}\frac{\int_0^L \phi_i(x)^2\mathrm{d}x}{U}. \end{aligned} \tag{10}$$

Equations (7)–(9) can be rewritten as

$$\begin{aligned} \mathbf{M}x + \mathbf{C}\dot{x} + \mathbf{K}x &= \mathbf{F}, \\ \mathbf{M} &= \begin{bmatrix} M_i + \mu M_i\phi_i(a)^2 & 0 & \mu M_i\phi_i(a) \\ (\mu+\beta)\phi_i(a) & -\beta & \mu+\beta \\ -\beta\phi_i(a) & \beta & -\beta \end{bmatrix}, \\ \mathbf{C} &= \begin{bmatrix} 2M_i\omega_i(\xi_i - \xi_{\mathrm{ae}}) & 0 & 0 \\ 0 & 0 & 0 \\ -2\mu\xi_T\omega_S\phi_i(a) & 2\mu\xi_T\omega_S & 0 \end{bmatrix}, \\ \mathbf{K} &= \begin{bmatrix} \left(M_i\omega_i^2 - K_{\mathrm{ae}}\right) & 0 & 0 \\ 0 & 0 & \mu\omega_s^2 \\ -\mu\omega_T^2\phi_i(a) & \mu\omega_T^2 & 0 \end{bmatrix}, \\ \mathbf{F} &= \begin{bmatrix} 1 \\ 0 \\ 0 \end{bmatrix}F_i, \\ \mathbf{x} &= \begin{bmatrix} q_i(t) \\ y_2(t) \\ y_t(t) - \phi_i(a)q_i(t) \end{bmatrix}, \end{aligned} \tag{11}$$

where $y_t - \phi_i(a)q_i(t)$ is the suspension travel. The mass matrix $\mathbf{M}$, the damping matrix $\mathbf{C}$, the stiffness matrix $\mathbf{K}$, and displacement vector $\mathbf{x}$ of other arrangements are as follows:

(1) C3 arrangement:

$$\mathbf{M}=\begin{bmatrix} M_i+\mu M_i\phi_i(a)^2 & 0 & 0 & \mu M_i\phi_i(a) \\ \phi_i(a) & 0 & 0 & 1 \\ 0 & \beta & -\beta & 0 \\ 0 & \beta & -\beta & 0 \end{bmatrix},$$

$$\mathbf{C}=\begin{bmatrix} 2M_i\omega_i(\xi_i-\xi_{ae}) & 0 & 0 & 0 \\ 0 & 0 & 0 & 0 \\ 2\mu\xi_T\omega_S\phi_i(a) & 0 & -2\mu\xi_T\omega_S & 2\mu\xi_T\omega_S \\ 0 & 0 & 0 & 0 \end{bmatrix},$$

$$\mathbf{K}=\begin{bmatrix} M_i\omega_i^2-K_{ae} & 0 & 0 & 0 \\ -\omega_T^2\phi_i(a) & \omega_T^2 & 0 & \omega_s^2 \\ 0 & 0 & 0 & 0 \\ -\mu\omega_T^2\phi_i(a) & \mu\omega_T^2 & 0 & 0 \end{bmatrix}, \tag{12}$$

$$\mathbf{x}=\begin{bmatrix} q_i(t) \\ y_2(t) \\ y_3(t) \\ y_t(t)-\phi_i(a)q_i(t) \end{bmatrix}.$$

(2) C5 arrangement:

$$\mathbf{M}=\begin{bmatrix} M_i+\mu M_i\phi_i(a)^2 & 0 & \mu M_i\phi_i(a) \\ \phi_i(a) & 0 & 1 \\ -\beta\phi_i(a) & \beta & 0 \end{bmatrix},$$

$$\mathbf{C}=\begin{bmatrix} 2M_i\omega_i(\xi_i-\xi_{ae}) & 0 & 0 \\ 2\xi_T\omega_S\phi_i(a) & -2\xi_T\omega_S & 2\xi_T\omega_S \\ -2\mu\xi_T\omega_S\phi_i(a) & 2\mu\xi_T\omega_S & -2\mu\xi_T\omega_S \end{bmatrix}$$

$$\mathbf{K}=\begin{bmatrix} \left(M_i\omega_i^2-K_{ae}\right) & 0 & 0 \\ 0 & 0 & \omega_s^2 \\ -\mu\omega_T^2\phi_i(a) & \mu\omega_T^2 & 0 \end{bmatrix}, \tag{13}$$

$$\mathbf{x}=\begin{bmatrix} q_i(t) \\ y_2(t) \\ y_t(t)-\phi_i(a)q_i(t) \end{bmatrix}.$$

(3) C6 arrangement:

$$\mathbf{M}=\begin{bmatrix} M_i+\mu M_i\phi_i(a)^2 & 0 & \mu M_i\phi_i(a) \\ \phi_i(a) & 0 & 1 \\ \beta\phi_i(a) & -\beta & 0 \end{bmatrix},$$

$$\mathbf{C}=\begin{bmatrix} 2M_i\omega_i(\xi_i-\xi_{ae}) & 0 & 0 \\ 0 & 0 & 0 \\ 2\mu\xi_T\omega_S\phi_i(a) & -2\mu\xi_T\omega_S & 0 \end{bmatrix},$$

$$\mathbf{K}=\begin{bmatrix} \left(M_i\omega_i^2-K_{ae}\right) & 0 & 0 \\ \omega_T^2\phi_i(a) & -\omega_T^2 & \omega_T^2+\omega_S^2 \\ \mu\omega_T^2\phi_i(a) & -\mu\omega_T^2 & \mu\omega_T^2 \end{bmatrix}, \tag{14}$$

$$\mathbf{x}=\begin{bmatrix} q_i(t) \\ y_2(t) \\ y_t(t)-\phi_i(a)q_i(t) \end{bmatrix}.$$

(4) C7 arrangement:

$$\mathbf{M}=\begin{bmatrix} M_i+\mu M_i\phi_i(a)^2 & 0 & \mu M_i\phi_i(a) \\ \mu\phi_i(a) & 0 & \mu+\beta \\ 0 & 0 & 0 \end{bmatrix},$$

$$\mathbf{C}=\begin{bmatrix} 2M_i\omega_i(\xi_i-\xi_{ae}) & 0 & 0 \\ 0 & 0 & 0 \\ 2\xi_T\omega_S\phi_i(a) & -2\xi_T\omega_S & 2\xi_T\omega_S \end{bmatrix},$$

$$\mathbf{K}=\begin{bmatrix} \left(M_i\omega_i^2-K_{ae}\right) & 0 & 0 \\ -\mu\omega_T^2\phi_i(a) & \mu\omega_T^2 & \mu\omega_S^2 \\ \omega_T^2\phi_i(a) & -\omega_T^2 & 0 \end{bmatrix}, \tag{15}$$

$$\mathbf{x}=\begin{bmatrix} q_i(t) \\ y_2(t) \\ y_t(t)-\phi_i(a)q_i(t) \end{bmatrix}.$$

(5) C8 arrangement:

$$\mathbf{M} = \begin{bmatrix} M_i + \mu M_i \phi_i(a)^2 & 0 & \mu M_i \phi_i(a) \\ \phi_i(a) & 0 & 1 \\ \beta \phi_i(a) & -\beta & \beta \end{bmatrix},$$
$$\mathbf{C} = \begin{bmatrix} 2M_i \omega_i (\xi_i - \xi_{ae}) & 0 & 0 \\ 0 & 0 & 2\xi_T \omega_S \\ 0 & 0 & 0 \end{bmatrix},$$
$$\mathbf{K} = \begin{bmatrix} \left(M_i \omega_i^2 - K_{ae}\right) & 0 & 0 \\ -\omega_T^2 \phi_i(a) & \omega_T^2 & \omega_s^2 \\ \mu \omega_T^2 \phi_i(a) & -\mu \omega_T^2 & 0 \end{bmatrix}, \quad (16)$$
$$\mathbf{x} = \begin{bmatrix} q_i(t) \\ y_2(t) \\ y_t(t) - \phi_i(a) q_i(t) \end{bmatrix}.$$

3. Determining the Performance Index with the Root Mean Square of the Displacement

It is noted that equations (11)–(16) are nonlinear equations, and they will be linearized in the following. According to the research of vortex-induced vibration based on a circular cylinder in [29], when in the "lock in" region of vortex-induced vibration, the aerodynamic damping ratio ξ_{ae} can be expressed as a function of the RMS σ_i. The relationship between ξ_{ae} and σ_i is as follows:

$$\xi_{ae} = K_a \frac{\rho D^2}{\rho_b A} \left[1 - \left(\frac{\sigma_i}{D a_L}\right)^2\right],$$
$$\frac{K_a}{K_{a\_max}} = \frac{0.9}{\left((U/U_{cr}) - 0.25\right)^2} e^{-1/\left((U/U_{cr})+0.02\right)^{24}} - 0.18, \quad (17)$$

where K_a is the linear aeroelastic damping parameter, K_{a_max} is the maximum value of K_a, a_L is the nonlinear aeroelastic damping parameter related to "lock in" phenomenon, and $U_{cr} = D f_i / S_t$ is the critical wind velocity.

The vortex-induced vibration applied to the bridge is periodic, and the vortex-induced vibration is a limiting vibration [1]. The change in RMS σ_i of $q_i(t)$ can be negligible and treated as a constant for an IDVA with given parameters. The relationship of parameters in (9) and (17) is as follows:

$$K_a = \frac{U Y_1}{4 \omega_i D},$$
$$a_L = \sqrt{\frac{2}{\varepsilon}} \sqrt{\frac{\int_0^L \phi_i(x)^2 \mathrm{d}x}{\int_0^L \phi_i(x)^4 \mathrm{d}x}}. \quad (18)$$

The aerodynamic damping ratio ξ_{ae} contains the unknown constant σ_i, the σ_i associated with different parameters for the same IDVA arrangement is different. Moreover, the input is not a white noise, and the method proposed by Jin et al. [26] is adopted.

With the application of the approximate expressions (17), for a given σ_i, equations (11)–(16) can be treated as a linear equation. Then, the frequency response functions of system are as follows:

$$\begin{bmatrix} H_i(\omega) \\ H_2(\omega) \\ H_T(\omega) \end{bmatrix} = \left[D_{Fcn}(\omega)^{-1}\right] \begin{bmatrix} 1 \\ 0 \\ 0 \end{bmatrix}, \quad (19)$$

where $D_{Fcn}(\omega) = -\omega^2 \mathbf{M} + \mathbf{K} + j\omega \mathbf{C}$, $j = \sqrt{-1}$ is the imaginary number, $H_i(\omega)$ is the frequency response function, and $H_2(\omega)$ and $H_T(\omega)$ are related to the displacement of the IDVA system. The power spectral density functions of the vertical displacement of the bridge $S_i(\omega)$ and the suspension travel $S_{sus}(\omega)$ can be obtained as

$$\begin{bmatrix} S_i(\omega) \\ S_{sus}(\omega) \end{bmatrix} = \begin{bmatrix} H_i^*(\omega) H_i(\omega) \\ H_T^*(\omega) H_T(\omega) \end{bmatrix} S_F(\omega), \quad (20)$$

where $H_i^*(\omega)$ is the conjugate of $H_i(\omega)$, $H_T^*(\omega)$ is the conjugate of $H_T(\omega)$, and $S_F(\omega)$ is the power spectral density of the excitation F_i. The power spectral density function of F_i is as follows [30]:

$$S_F(\omega) = \frac{2 {q_v}^2 D^3 \sigma_{CL}^2 \lambda}{\sqrt{\pi} f_s B} e^{-\left(1 - \left((\omega/\omega_s)/B\right)\right)} \int_0^L \phi_i(x)^2 \mathrm{d}x, \quad (21)$$

where $q_v = \rho U^2/2$ is the wind pressure, ρ is the air density, σ_{CL} is the RMS of the lift coefficient, $f_s = U S_t / D$ ($\omega_s = 2\pi f_s$) is the vortex-shedding frequency, S_t is the Strouhal number, B is the load spectrum bandwidth, and λ is a dimensionless parameter related to the coherence function.

Performance index J related to the vertical displacement of the bridge and performance index J_s related to the suspension travel are defined as follows:

$$J = \frac{\sigma_i}{D} = \sqrt{\frac{\int_{-\infty}^{+\infty} S_i(\omega) \mathrm{d}\omega}{2\pi D^2}},$$
$$J_s = \frac{\sigma_{sus}}{D} = \sqrt{\frac{\int_{-\infty}^{+\infty} S_{sus}(\omega) \mathrm{d}\omega}{2\pi D^2}}. \quad (22)$$

For an IDVA with given parameters, the performance index J can be obtained by an iterative method [21]. Assume that $\xi_{ae} = K_a (\rho D^2 / \rho_b A)[1 - (\sigma_0 / D a_L)]^2$. In order to ensure the convergence of results, the stability of the bridge-IDVA system is considered, which is checked by

$$\det\left(\mathbf{M}\lambda^2 + \mathbf{C}\lambda + \mathbf{K}\right) = 0, \quad (23)$$

where the eigenvalues of (23) are λ_k, $k = 1, \ldots, n$; n is the number of the eigenvalues. The real part of all eigenvalues should be less than 0. Therefore, the following condition applies:

$$\max\left[\mathrm{Re}\left(\lambda_k\right)\right] < 0. \tag{24}$$

The detailed iterative process is shown in Figure 8. First, let the $\sigma_0 = 0$, and the number of initial iterations is $N = 50$, which reduced by one in each iteration process. Substitute $\sigma_0$into the equation to calculate σ_i. The performance index J can be obtained if the system is stable and $(|\sigma_0 - \sigma_i|/\sigma_i) < 1\%$. If $(|\sigma_0 - \sigma_i|/\sigma_i) > 1\%$, σ_i will be assigned to σ_0. And the next iteration process will be repeated. If the system is not stable, output $J = 1$. After the output of the performance index J, the next set of IDVA parameters will be the input and the iterative process is repeat. This iterative method can effectively avoid the problem of calculation falling into an infinite loop when the system diverges. An optimization problem to minimize the performance index J is formulated and solved by using the fmincon function in MATLAB. The optimization tool cannot obtain the theoretical optimal solution. In this paper, the error of the optimal parameters is reduced by increasing the number of iterations.

4. Case Study

4.1. The Structural Parameters and Aerodynamic Parameters. The case of the Osteroy suspension bridge in Norway is studied. Table 1 lists the structural parameters, the selected mode which resonates with the wind load can be obtained by a wind tunnel test, this mode represents the bending motion of a bridge, and it is the second symmetric mode of the bridge [30, 31]. This mode is selected because it has the most vortex vibrations, the longest occurrence time, and the largest vibration amplitude among all modes [31]. As the focus of this paper is not to obtain the resonance mode, the mode in this paper is quoted from the existing literature, so as to illustrate the correctness of the results in this paper.

Table 2 lists the aerodynamic parameters [30]. The simulation result during 8000 seconds without any controller shows the relationship between the RMS of the reduced bridge displacement and the reduced wind velocity $U/(Df_i)$ in Figure 9(a). When the reduced wind velocity $U/(Df_i)$ is about 6.63, the reduced RMS of the bridge displacement reaches maximum; the uncontrolled case is shown in Figure 9(b).

4.2. The Optimal Installation Position of the IDVA. In this section, the optimization of the IDVA system is considered, including the optimal installation position and the optimal parameters of the IDVA. When studying the IDVA installation location, the effects of the bridge structural damping, the vortex-induced aerodynamic damping and the aerodynamic stiffness are ignored. Combining the empirical nonlinear model proposed by Ehsan and Scanlan [32], the vortex-induced force is simplified into a simple harmonic distributed excitation; then (2) can be simplified as

$$\begin{gathered}\rho_b A\frac{\partial^2 y_1(x,t)}{\partial t^2} + m_{\mathrm{IDVA}}\frac{\partial^2 y_t(t)}{\partial t^2}\delta(x-a) + EI\frac{\partial^4 y_1(x,t)}{\partial x^4} = F_{\mathrm{wind\_a}},\\ F_{\mathrm{wind\_a}} = \frac{1}{2}\rho U^2 D f(x)\widetilde{C}_L \sin\left(\omega_i t + \varphi\right),\end{gathered} \tag{25}$$

where $f(x)$ is the excitation distribution function and φ is the initial phase. Derived from the equation of motion of controller, we can obtain

$$-m_{\mathrm{IDVA}}\omega^2 y_t = \left[K_s + j\omega Y(j\omega)\right]\left(y_1(a,\omega) - y_t\right), \tag{26}$$

where $Y(j\omega)$ is the admittance function of any IDVA and $j = \sqrt{-1}$.

Substitute (6) into (25), and multiply both sides of the equation by $\phi_i(x)$, and then integrate x from *0* to L. After a dimensionless calculation process, one can obtain

$$\begin{gathered}M_i\ddot{q}_i(t) + \mu M_i\phi_i(a)\ddot{y}_t + M_i\omega_i^2 q_i(t) = F_{\mathrm{wind\_a}},\\ F_{\mathrm{wind\_a}} = \frac{1}{2}\rho U^2 D\widetilde{C}_L\int_0^L f(x)\phi_i(x)\mathrm{d}x\sin\left(\omega_i t + \varphi\right).\end{gathered} \tag{27}$$

After applying the Fourier transform to (27), the frequency response function of the system is

$$\begin{gathered}H(\omega) = \frac{1}{M_i\omega_i^2 - \omega^2 M_i - \omega^2\mu M_i\phi_i(a)^2 G(j\omega)},\\ G(j\omega) = \frac{K_s + j\omega Y(j\omega)}{K_s - m_{\mathrm{IDVA}}\omega^2 + j\omega Y(j\omega)}.\end{gathered} \tag{28}$$

According to (28), the suppression performance of IDVA in $\phi_i(a)$ is the same as the one in $-\phi_i(a)$, and $\phi_i(a)$ is selected greater than 0 in the following analysis. Then,

$$G(j\omega) = R_Y(\omega) + I_Y(\omega)j, \tag{29}$$

where $R_Y(\omega)$ is the real part of $G(j\omega)$ and $I_Y(\omega)$ is the imaginary part of $G(j\omega)$, and (28) can be written.

The performance index related to the vertical displacement of the bridge J_a is

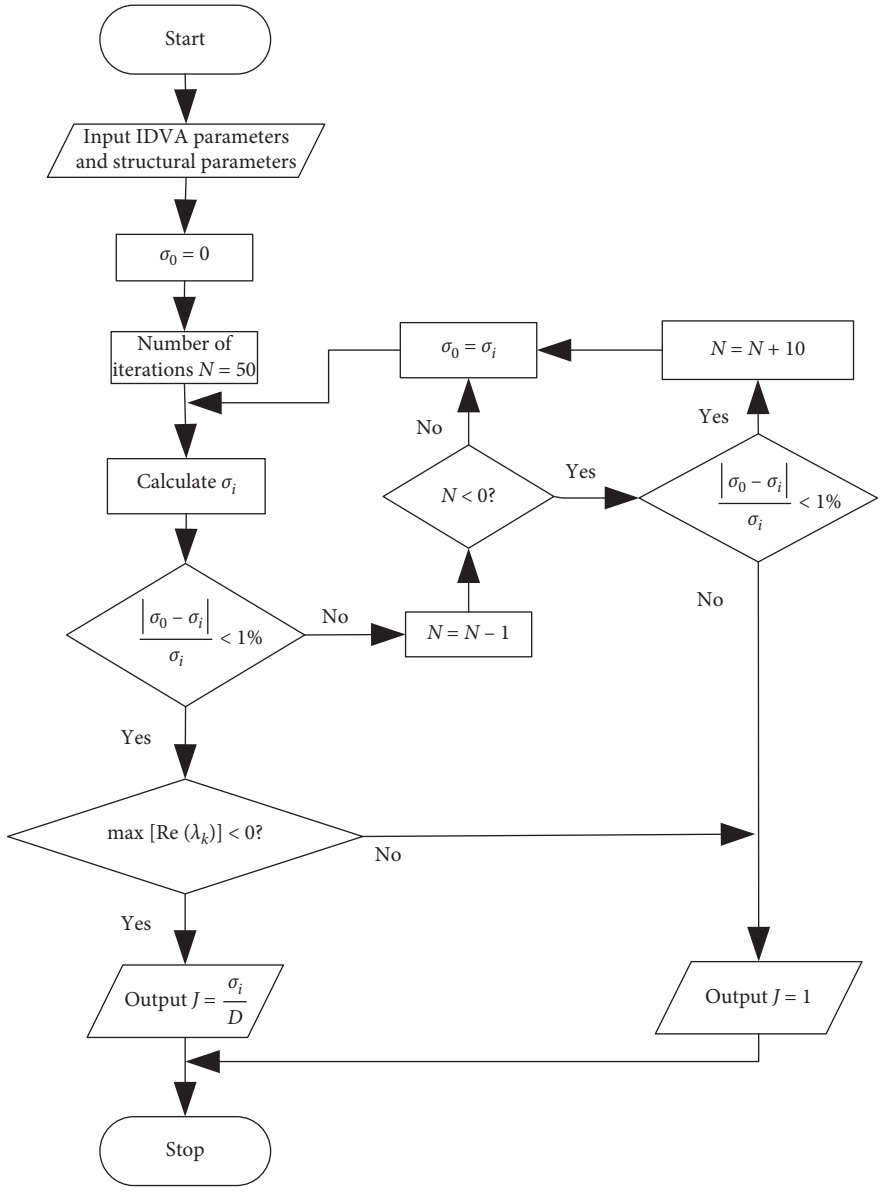

Figure 8: The method to calculate performance index with the given IDVA parameter.

Table 1: The structural parameters.

L (m)	$\rho_b A$	D (m)	$\phi_i(\mathbf{x})$	f_i	ξ_i
595	7460 kg/m	2.5	$\sin(4\pi x/L)$	0.391 Hz	0.24%

Table 2: The relevant aerodynamic parameters.

S_t	a_L	$\sigma_{CL}^2 \lambda/B$	B	$K_{\max}$	K_a	$U = 1.06U_{cr}$	$U_{cr} = Df_i/S_t$
0.16	0.233	15.3664	0.2	2.43	2.41	6.4925	6.125

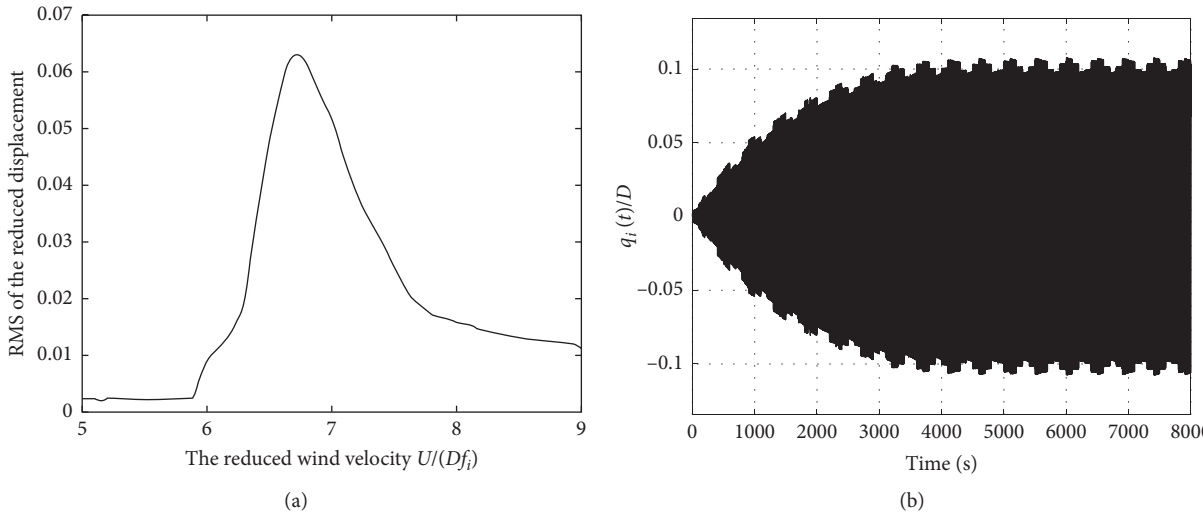

(a) (b)

Figure 9: The uncontrolled response. (a) The relationship between the RMS of the reduced bridge displacement and the reduced wind velocity; (b) simulation result when $U = 1.06U_{cr}$.

$$J_a = \sqrt{\frac{W(a)}{4D^2}\left(\frac{1}{2}\rho U^2 D\widetilde{C}_L \int_0^L f(x)\phi_i(x)\mathrm{d}x\right)^2},$$
$$W(a) = \frac{1}{\omega_i^4 \mu^2 M_i^2 \phi_i(a)^4}\left(\frac{1}{R_Y(\omega_i)^2 + I_Y(\omega_i)^2} + \frac{1}{R_Y(-\omega_i)^2 + I_Y(-\omega_i)^2}\right). \tag{30}$$

From (30), it is observed that the performance index J_a is the smallest as $W(a)$ reaches the minimum, so the optimal installation position of the controller must meet the condition:

$$\left|\phi_i(a)\right| = 1. \tag{31}$$

The optimal installation position indicated in (31) is just the maximum of the modal displacement. According to (26), the admittance function of any IDVA is a general expression, which also means that the conclusion of (31) is not only applicable to IDVA systems, but also to any passive controller.

The effect of the installation position for IDVAs on the performance index J and the optimal parameters will be studied with the ignored factors as before. During optimization process, the mass ratio μ is selected as 0.1 and four different values of $\phi_i(a)$ are selected. The performance of IDVA is nonlinear with respect to $\phi_i(a)$. We obtain denser sample points near $|\phi_i(a)| = 1$, and four sample points are sufficient to illustrate the research results of this paper.

As shown in Figure 10, the inertance-to-mass ratio β, the corner frequency ratio ω_T/ω_s, and the damping ratio ξ_T of C3-C7 arrangements all increase as $\phi_i(a)$ increases, except the natural frequency ratio ω_s/ω_i. The inertance-to-mass ratio β of the C8 arrangement is too large and not shown; its corner frequency ratio ω_T/ω_s decreases with the increase of $\phi_i(a)$. It can be concluded that the installation position of the IDVAs has a great impact on the optimal parameters of IDVAs.

As shown in Figure 11, the performance of the C3-C8 arrangements in suppressing the vortex-induced vibration is better with a larger $\phi_i(a)$, which is consistent with the conclusion in (31). As shown in Figure 12, due to the resonant mode corresponding to the observed number of half-waves being four, there are four suitable installation positions for any IDVA which can be located at $L/8$, $(3L/8)$, $(5L/8)$, and $(7L/8)$. Therefore, IDVAs should be installed at the maximum modal displacement.

4.3. IDVA Optimal Parameter Optimization and Performance Comparison. Take $\Phi_i(a) = 1$ to determine the installation positions of IDVA; then use MATLAB's optimization tools to obtain the optimal parameters and performance indexes of C3-C8 arrangements under the given mass ratio μ; seven mass ratios are selected from 0 to 0.1 before the analysis. The mass ratio μ should be an input-determined parameter before the analysis, because the ancillary mass on the bridge is limited. Usually, the ancillary mass cannot exceed 10% of the mass of the bridge. Inerter has the effect of amplifying its own mass; therefore the mass of the inerter occupies a small part of the auxiliary mass, and it is not necessary to determine inertance-to-mass ratio β before the analysis.

The reasonable stiffness is also considered; the stiffness is converted into a dimensionless parameter, such as the natural frequency $\omega_s = \sqrt{K_s/m_{\mathrm{IDVA}}}$ and the corner frequency $\omega_T = \sqrt{k_{\mathrm{IDVA}}/m_{\mathrm{IDVA}}}$. In general, the values of the

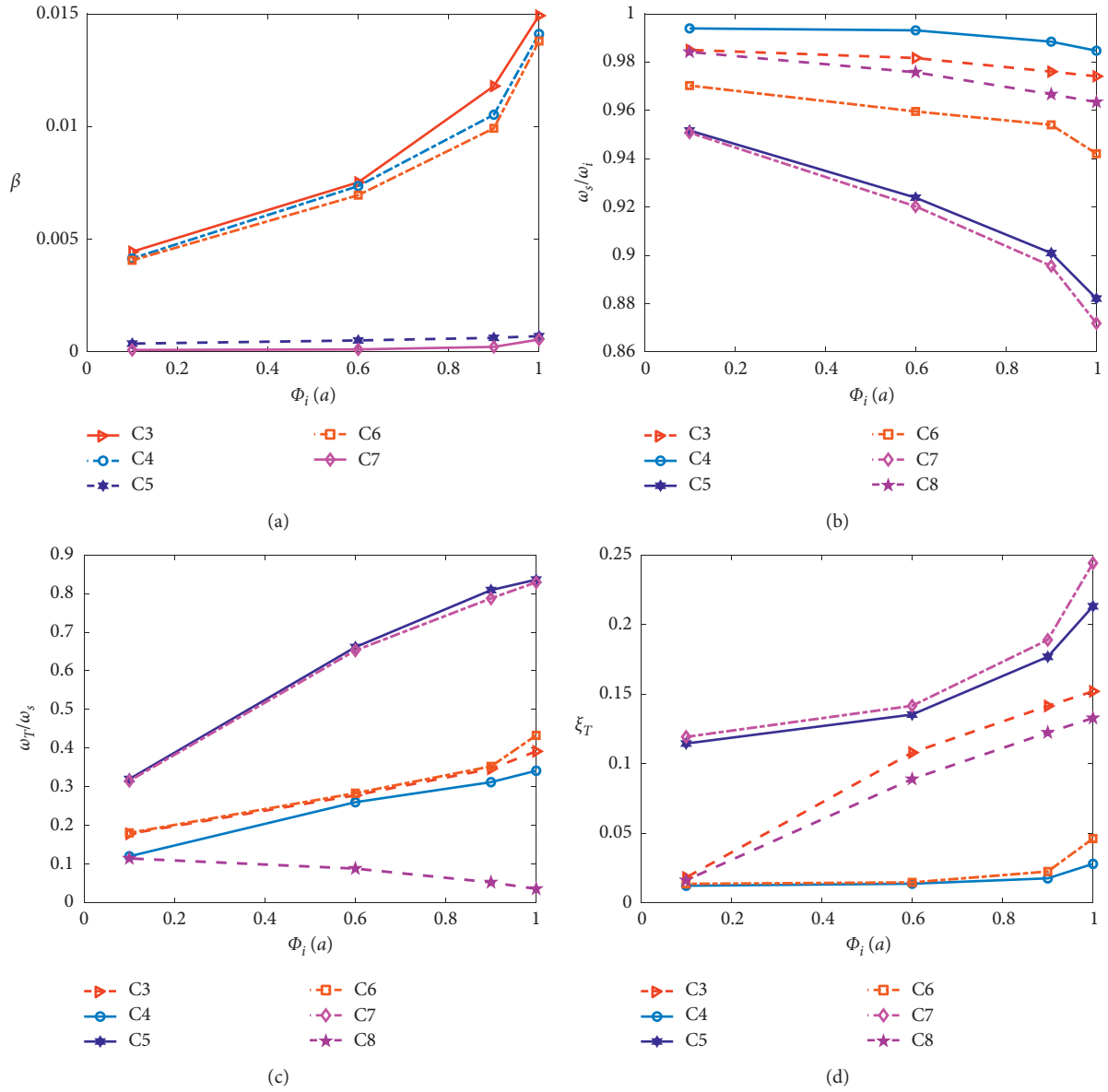

FIGURE 10: Effect of installation position on optimal parameters. (a) The inertance-to-mass ratio β, (b) the natural frequency ratio ω_s/ω_i, (c) the corner frequency ratio ω_T/ω_s, and (d) the damping ratio ξ_T.

natural frequency ratio ω_s/ω_i and the corner frequency ratio ω_T/ω_s are selected from 0 to 1.

The effect of the mass ratio μ on the optimal parameters is shown in Figure 13. As the mass ratio μ increases, the inertance-to-mass ratio β, the corner frequency ratio ω_T/ω_s, and the damping ratio ξ_T of all arrangements increase, except the natural frequency ratio ω_s/ω_i. The inertance-to-mass ratio β of C5 and C7 arrangements is much smaller than the others and their corner frequency ratios ω_T/ω_s are much larger than the others, which is opposite to the C8 arrangement.

The optimal damping ratio ξ_{TDVA} and the optimal natural frequency ω_{TDVA} of the traditional dynamic vibration absorber (TDVA) to suppress vortex-induced vibration [30] are

$$\omega_{\mathrm{TDVA}} = \frac{\omega_i}{\sqrt{1+1.5\mu}},$$
$$\xi_{\mathrm{TDVA}} = \sqrt{0.25\mu\,(1-0.75\mu)}. \tag{32}$$

In order to show the error between IDVA performance and TDVA performance, we define the performance error

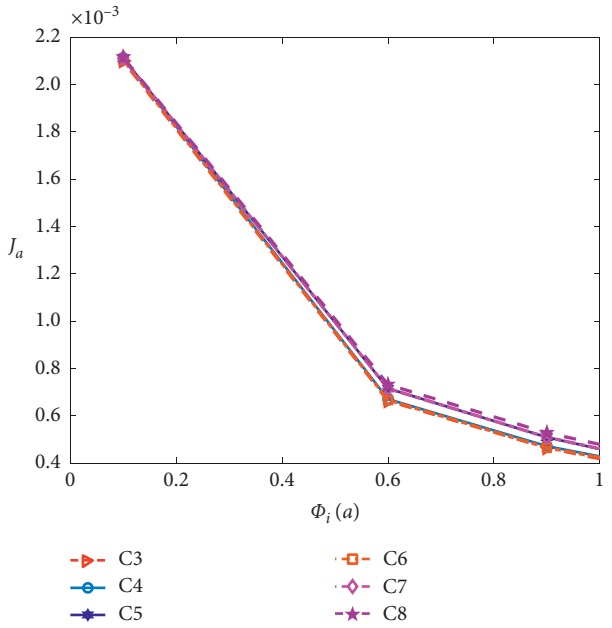

Figure 11: Effect of installation position on performance.

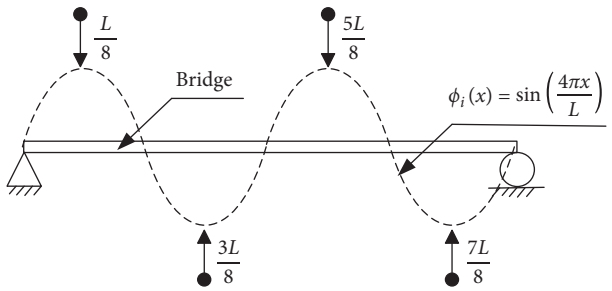

Figure 12: The installation positions of IDVA.

indexes of vortex-induced vibration suppression ΔJ and the suspension travel performance ΔJ_s.

$$\Delta J = \frac{\text{IDVA performance } J - \text{TDVA performance } J}{\text{TDVA performance } J} \times 100\%,$$
$$\Delta J_s = \frac{\text{IDVA performance } J_s - \text{TDVA performance } J_s}{\text{TDVA performance } J_s} \times 100\%. \tag{33}$$

Figure 14 mainly presents the effect of the mass ratio μ on the performance. It can be seen that the performance of the all arrangements in suppressing vortex-induced vibration is better when the mass ratio μ increases. Among them, C3 is the best arrangement, followed by C6 and C4, and then C5 and C7. C8 is the worst arrangement which is similar to TDVA. In terms of the suspension travel, the performance of the C3–C8 arrangements deteriorates. C5, C7, and C8 have less influence than other arrangements. C3 and C4 only improve the suspension travel when the mass ratio μ is 0.005.

5. Time Domain Analysis

The aerodynamic damping ξ_{ae} used in the optimization process is based on (17), which is a linear model based on the research conclusion of the vortex-induced force of a cylinder in [29]. The aerodynamic damping ξ_{ae} used in the following simulation is based on (10) and belongs to a nonlinear model. This paper uses simulation results to verify whether the linearization measure based on research results by Vickery and Basu [29] is reasonable during optimization,

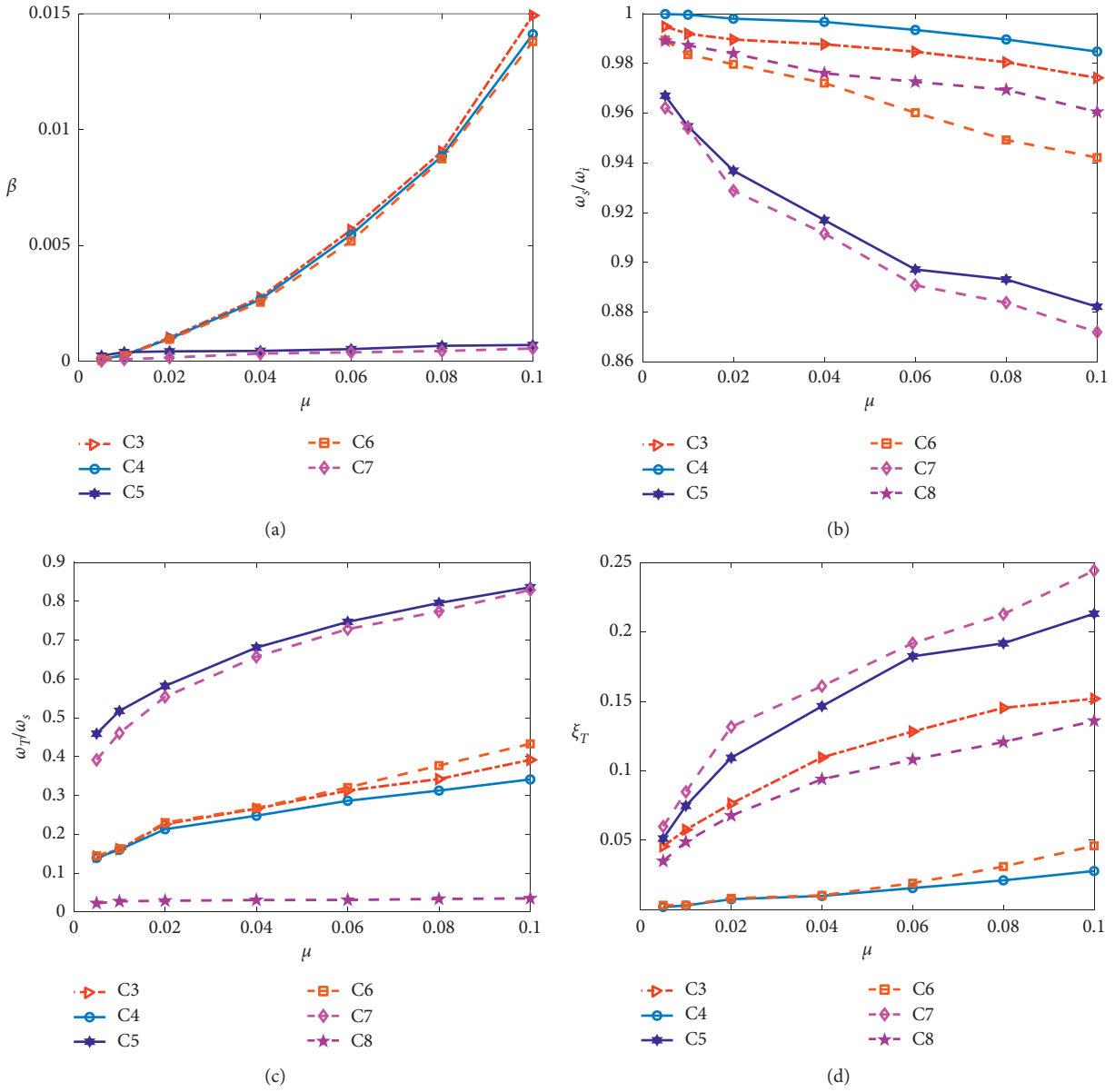

FIGURE 13: Effect of the mass ratio on optimal parameters. (a) The inertance-to-mass ratio β, (b) the natural frequency ratio ω_s/ω_i, (c) the corner frequency ratio ω_T/ω_s, and (d) the damping ratio ξ_T.

and compare the performance of C3–C8 arrangements in suppressing vortex-induced vibration.

In order to show the error between simulation performance and optimization performance, we define the performance error indices of vortex-induced vibration suppression ∇J and the suspension travel performance ∇J_s.

$$\nabla J = \frac{\text{optimization performance } J - \text{simulation performance } J}{\text{simulation performance } J} \times 100\%,$$
$$\nabla j_s = \frac{\text{optimization performance } J_s - \text{simulation performance } J_s}{\text{simulation performance } J_s} \times 100\%, \tag{34}$$

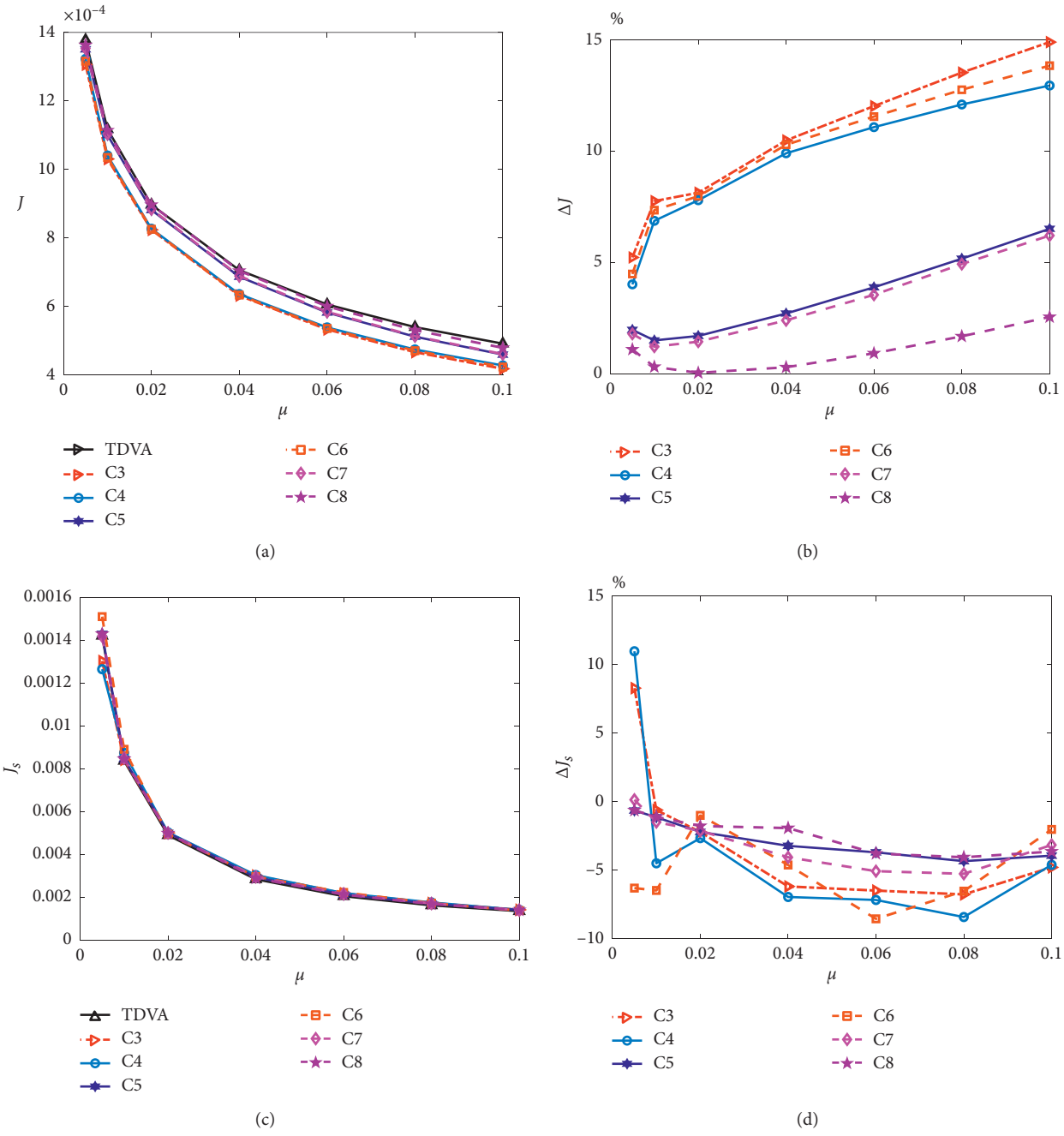

Figure 14: Effect of mass ratio on performance. (a) Displacement performance J, (b) performance improvement ΔJ with respect to TDVA, (c) suspension travel performance J_s, and (d) performance improvement $\Delta J_s$with respect to TDVA.

In the time-domain analysis, a time-domain signal $F_i$needs to be constructed, and its power spectral density function must satisfy S_F. The construction method adopts the method proposed by Shinozuka and Jan [33].

$$F_i = \sum_{l=1}^{N} \sqrt{2\Delta f} H_v(\omega_l) \cos(\omega_t + \theta_l), \tag{35}$$

where $H_v(\omega_l) = \sqrt{S_F(\omega_l)}$, $\omega_l = 2\pi l \Delta f$, $\Delta f = f_u/N_u$, $\theta_l \in [0, 2\pi]$, $f_u = 20$ Hz is the cut-off frequency, and $\Delta f = 0.01$ Hz is the frequency segment.

First, the effect of the IDVA installation position on the suppression of vortex-induced vibration is studied. The C3, C5, and C8 arrangements are selected, the mass ratio $\mu = 0.1$, and four different values of $\phi_i(a)$ are selected for simulation. The response is basically periodic; the simulation results of 100 seconds (from 90 seconds to 190 seconds) are shown. According to Figure 15, for the same IDVA arrangement, the performance of suppressing vortex-induced vibration is improved as $\phi_i(a)$ increases, which is consistent with the expected results. Therefore, the most suitable installation position for IDVA meets the condition that $|\phi_i(a)| = 1$.

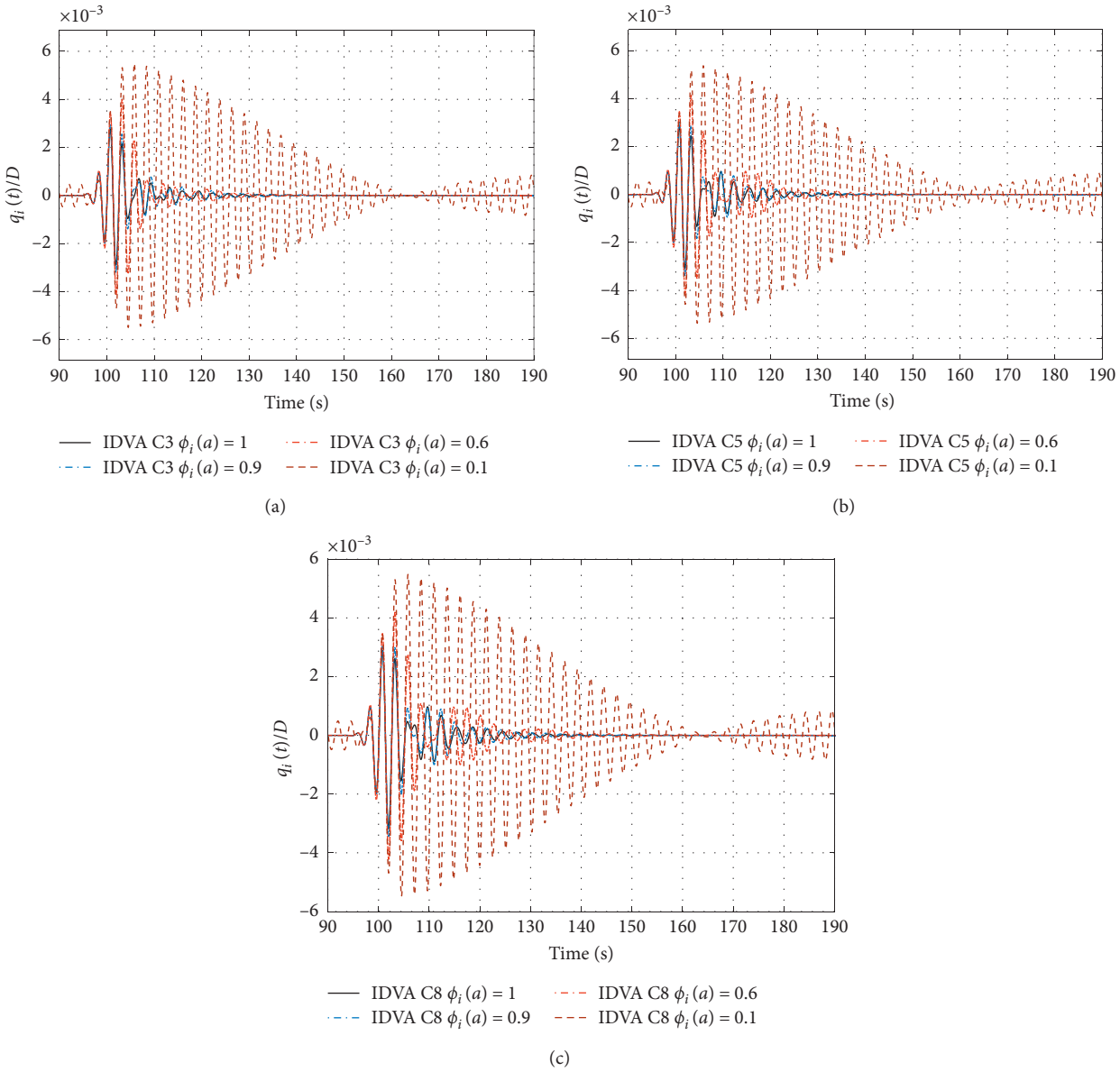

Figure 15: Simulation response for different installation positions. (a) C3. (b) C5. (c) C8.

After determining the installation position of IDVA, the performances of different IDVA arrangements to suppress vortex-induced vibration are compared. Two different mass ratios μ (0.005 and 0.1) are selected to compare for 8000 seconds simulation time. The simulation results of the C3-C8 arrangements and TDVA from 90 seconds to 190 seconds are shown in Figures 16 and 17. The statistical results are listed in Table 3.

From the simulation results, the comparative results of all arrangements in term of the performance index J are the same for all mass ratios. The C3 arrangement has the best performance in suppressing vortex-induced vibration, followed by C6 and C4, then C5 and C7, and the worst one is C8. In terms of the suspension travel compared with TDVA, when the mass ratio μ is 0.005, the improvement of C4 is the most obvious, followed by C3 and C7, and the other arrangements have degraded the suspension travel performance. When the mass ratio μ is 0.1, the suspension travel performance of the C3 arrangement deteriorates most significantly, and the C6 arrangement has the least impact. If the suspension travel margin is insufficient, C4 and C6 arrangements can replace the C3 arrangement.

The performance difference of C3-C8 arrangements is related to the given mass ratio μ; the mass ratio μ selected from 0 to 0.1 is widely accepted. Although the difference between C3–C8 is relatively small when the mass ratio μ is 0.005, the performance difference will gradually increase with the increasing mass ratio μ. Overall, C3 is the best.

According to Table 3, the error between the simulation results and the optimization results does not exceed 1.07%. It can be seen that it is reasonable to use the research results by Vickery and Basu [29] for linearization.

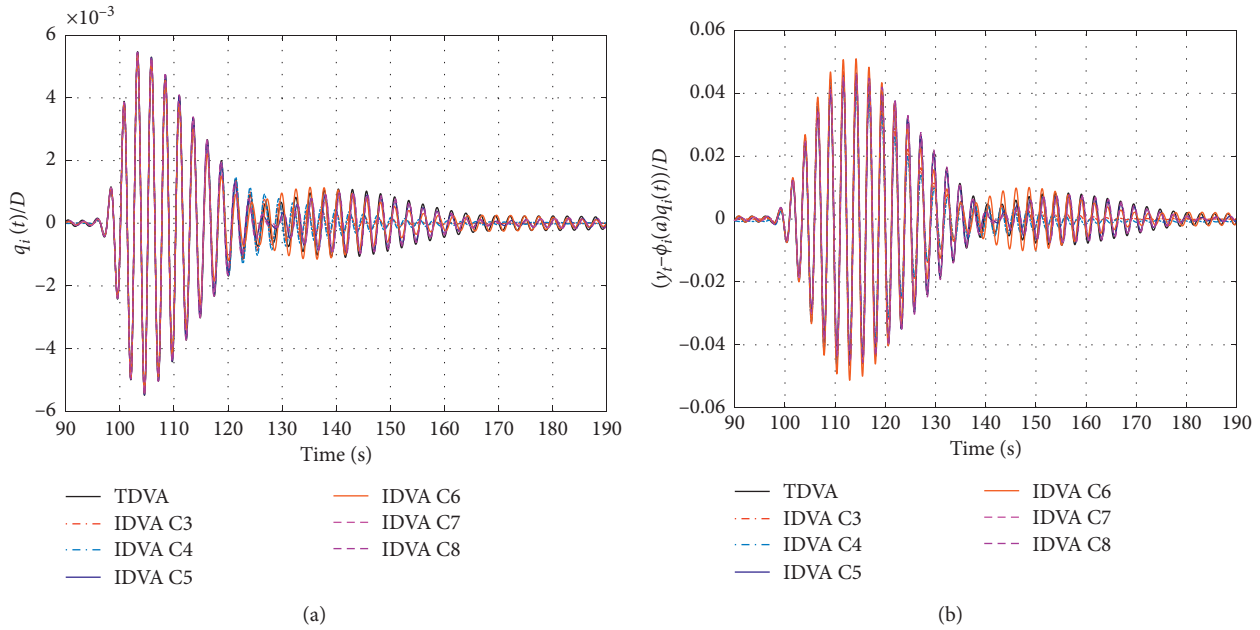

Figure 16: Simulation response of IDVAs and TDVA when mass ratio $\mu = 0.005$. (a) The reduced displacement; (b) the reduced suspension travel.

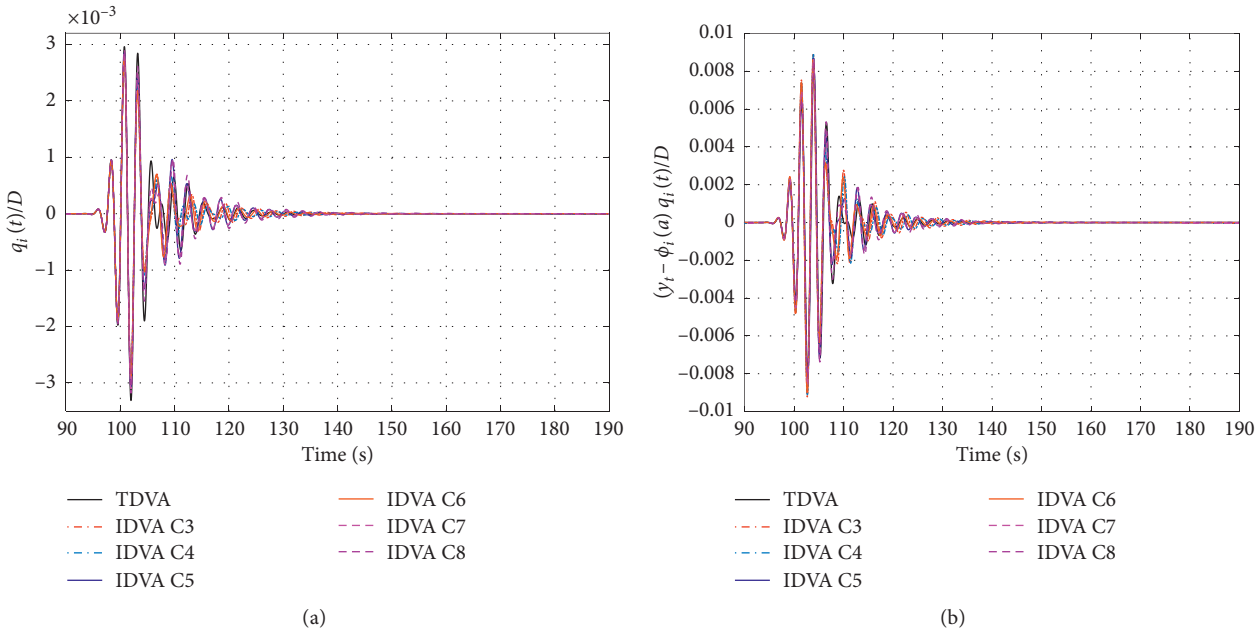

Figure 17: Simulation response of IDVAs and TDVA when mass ratio $\mu = 0.1$. (a) The reduced displacement; (b) the reduced suspension travel.

6. Conclusions

This paper mainly compares the performance of different IDVAs in suppressing vortex-induced vibration and comprehensively considers the effect of installation position on the suppression of vortex-induced vibration. Among the C3–C8 arrangements, the C3 arrangement has the best performance in suppressing vortex-induced vibration, followed by C6 and C4, and then C5 and C7, and the worst one is C8. In terms of the suspension travel, the performance of the C3–C8 arrangements deteriorates. C5, C7, and C8 have less influence than other arrangements. C3 and C4 only improve the suspension travel when the mass ratio μ is 0.005. According to the theoretical analysis and simulation results,

Table 3: Simulation results of IDVAs and TDVA.

μ	Arrangement	J	ΔJ	∇J	J_s	ΔJ_s	∇J_s
	C3	0.00129	5.91%	0.62%	0.01342	9.02%	0.07%
	C4	0.001302	5.03%	0.99%	0.0131	11.19%	0.71%
	C5	0.001338	2.41%	0.45%	0.01481	−0.41%	0.42%
0.005	C6	0.001293	5.69%	1.07%	0.01546	−4.81%	0.59%
	C7	0.001342	2.12%	0.37%	0.01471	0.27%	0.49%
	C8	0.00135	1.53%	0.44%	0.01477	−0.14%	−0.21%
	TDVA	0.001371	—	—	0.01475	—	—
	C3	0.000421	14.95%	0.29%	0.001428	−5.00%	0.07%
	C4	0.0004307	12.99%	0.26%	0.001418	−4.26%	0.36%
	C5	0.0004621	6.65%	0.31%	0.00141	−3.68%	0.29%
0.1	C6	0.0004263	13.88%	0.26%	0.001382	−1.62%	0.29%
	C7	0.0004637	6.32%	0.28%	0.00141	−3.68%	−0.43%
	C8	0.0004815	2.73%	0.38%	0.001407	−3.46%	0.36%
	TDVA	0.000495	—	—	0.00136	—	—

the optimal installation position of IDVA should be where the maximum of the modal displacement occurs, which can be applicable to any passive controller.

Data Availability

The data used to support the findings of this study are available from the corresponding author upon request.

Conflicts of Interest

The authors declare that they have no conflicts of interest.

Acknowledgments

This research was supported by the National Natural Science Foundation of China under Grant 61873129.

References

[1] Y. L. Xu, *Wind Effects on Cable-Supported Bridges*, John Wiley & Sons, Hoboken, NJ, USA, 2013.

[2] X. Du, Y. Zhao, G. Liu et al., "Enhancement of the piezoelectric cantilever beam performance via vortex-induced vibration to harvest ocean wave energy," *Shock and Vibration*, vol. 2020, Article ID 8858529, 11 pages, 2020.

[3] M. Zhang, T. Wu, and F. Xu, "Vortex-induced vibration of bridge decks: describing function-based model," *Journal of Wind Engineering and Industrial Aerodynamics*, vol. 195, Article ID 104016, 2019.

[4] M. Zhang, F. Xu, and O. Øiseth, "Aerodynamic damping models for vortex-induced vibration of a rectangular 4:1 cylinder: comparison of modeling schemes," *Journal of Wind Engineering and Industrial Aerodynamics*, vol. 205, Article ID 104321, 2020.

[5] S. Oh, S. Seo, H. Lee, and H. E. Lee, "Prediction of wind velocity to raise vortex-induced vibration through a road-rail bridge with truss-shaped girder," *Shock and Vibration*, vol. 2018, Article ID 2829640, 10 pages, 2018.

[6] S. B. Tao, A. P. Tang, D. B. Xin, K. T. Liu, and H. F. Zhang, "Vortex-induced vibration suppression of a circular cylinder with vortex generators," *Shock and Vibration*, vol. 2016, Article ID 5298687, 10 pages, 2016.

[7] M. T. Song, D. Q. Cao, and W. D. Zhu, "Vortex-induced vibration of a cable-stayed bridge," *Shock and Vibration*, vol. 2016, Article ID 1928086, 14 pages, 2016.

[8] Z. Zhou, T. Yang, Q. Ding, and Y. Ge, "Mechanism on suppression in vortex-induced vibration of bridge deck with long projecting slab with countermeasures," *Wind and Structures*, vol. 20, pp. 643–660, 2015.

[9] D. Xin, H. Zhang, and J. Ou, "Experimental study on mitigating vortex-induced vibration of a bridge by using passive vortex generators," *Journal of Wind Engineering and Industrial Aerodynamics*, vol. 175, pp. 100–110, 2018.

[10] C. B. Ronaldo and S. P. Michele, "Reduction of vortex-induced oscillations of Rio-Niteroi bridge by dynamic control devices," *Journal of Wind Engineering and Industrial Aerodynamics*, vol. 84, no. 3, pp. 273–288, 2000.

[11] Y. Fujino and Y. Yoshida, "Wind-induced vibration and control of trans-Tokyo Bay crossing bridge," *Journal of Structural Engineering*, vol. 128, no. 8, pp. 1012–1025, 2002.

[12] Z. Huang and Z. Chen, "Application of multiple tuned mass damper for higher-order vortex-induced vibration of suspension bridge with steel box girder," *Journal of Vibration Engineering*, vol. 26, no. 6, pp. 908–914, 2013.

[13] M. C. Smith, "Synthesis of mechanical networks: the inerter," *IEEE Transactions on Automatic Control*, vol. 47, no. 10, pp. 1648–1662, 2002.

[14] M. Z. Q. Chen and Y. Hu, *Inerter and its Application in Vibration Control Systems*, Springer, Singapore, 2019.

[15] M. Z. Q. Chen, K. Wang, and G. Chen, *Passive Network Synthesis: Advances with Inerter*, World Scientific, Singapore, 2020.

[16] Y. Hu, M. Z. Q. Chen, S. Xu, and Y. Liu, "Semi-active inerter and its application in adaptive tuned vibration absorbers," *IEEE Transactions on Control Systems Technology*, vol. 25, no. 1, pp. 294–300, 2017.

[17] J. Luo, J. Z. Jiang, and J. H. G. Macdonald, "Damping performance of taut cables with passive absorbers incorporating inerters," *Journal of Physics: Conference Series*, vol. 744, Article ID 012046, 2016.

[18] J. Luo, J. H. G. Macdonald, and J. Z. Jiang, "Use of inerter-based vibration absorbers for suppressing multiple cable modes," *Procedia Engineering*, vol. 199, pp. 1695–1700, 2017.

[19] J. Luo, J. Z. Jiang, and J. H. G. Macdonald, "Cable vibration suppression with inerter-based absorbers," *Journal of Engineering Mechanics*, vol. 145, no. 2, Article ID 04018134, 2019.

[20] J. Luo, J. H. G. Macdonald, and J. Z. Jiang, "Identification of optimum cable vibration absorbers using fixed-sized-inerter layouts," *Mechanism and Machine Theory*, vol. 140, pp. 292–304, 2019.

[21] K. Xu, K. Bi, Q. Han et al., "Using tuned mass damper inerter to mitigate vortex-induced vibration of long-span bridges: analytical study," *Engineering Structures*, vol. 182, pp. 101–111, 2019.

[22] J. Dai, Z. D. Xu, and P. P. Gai, "Tuned mass-damper-inerter control of wind-induced vibration of flexible structures based on inerter location," *Engineering Structures*, vol. 199, Article ID 109585, 2019.

[23] Y. Hu and M. Z. Q. Chen, "Performance evaluation for inerter based dynamic vibration absorbers," *International Journal of Mechanical Sciences*, vol. 99, pp. 297–307, 2015.

[24] Y. Sugimura, W. Goto, H. Tanizawa, K. Saito, and T. Nimomiya, "Response control effect of steel building structure using tuned viscous mass damper," in *Proceedings of the 15th World Conference on Earthquake Engineering*, Lisbon, Portugal, September 2012.

[25] K. Xu, K. Bi, Y. Ge et al., "Performance evaluation of inerter-based dampers for vortex-induced vibration control of long-span bridges: a comparative study," *Structural Control and Health Monitoring*, vol. 27, no. 6, Article ID e2529, 2020.

[26] X. Jin, M. Z. Q. Chen, and Z. Huang, "Suppressing random response of a regular structure by an inerter based dynamic vibration absorber," *Journal of Vibration and Acoustics*, vol. 141, no. 4, Article ID 041004, 2019.

[27] F. Cao, M. Z. Q. Chen, and Y. Hu, "Seismic isolation performance evaluation for a class of inerter - based low-complexity isolators," *Shock and Vibration*, vol. 2020, Article ID 8837822, 12 pages, 2020.

[28] G. Fairweather, *Finite Element Galerkin Methods for Differential Equations*, Marecl Dekker Inc, New York, NY, USA, 1978.

[29] B. J. Vickery and R. I. Basu, "Across-wind vibrations of structures of circular cross-section part I, development of a mathematical model for two-dimensional conditions," *Journal of Wind Engineering and Industrial Aerodynamics*, vol. 12, no. 1, pp. 49–73, 1983.

[30] E. Strommen and E. Hjorth-Hansen, "On the use of tuned mass dampers to suppress vortex shedding induced vibrations," *Wind and Structures*, vol. 4, no. 1, pp. 19–30, 2001.

[31] B. Isaksen, E. Strommen, and K. Gjerding-Smith, "Suppression of vortex shedding vibration at Osteroy suspension bridge," in *Proceedings of the Fourth Symposium on Strait Crossings*, Bergen, Norway, September 2001.

[32] F. Ehsan and R. H. Scanlan, "Vortex-induced vibrations of flexible bridges," *Journal of Engineering Mechanics*, vol. 116, no. 6, pp. 1392–1411, 1990.

[33] M. Shinozuka and C. M. Jan, "Digital simulation of random processes and its applications," *Journal of Sound and Vibration*, vol. 25, no. 1, pp. 111–128, 1972.